JGR Solid Earth

RESEARCH ARTICLE
10.1029/2020JB020519

Key Points:

- Underlying patterns in focal mechanisms can be revealed by an approach that combines unsupervised learning techniques
- The prevailing kinematics and stress regime are inferred by a spatial analysis and focal mechanisms categorization
- The tectonic regime characterizing key sectors of the studied region is identified

Supporting Information:

- Supporting Information S1

Correspondence to:
L. Scarfì,
luciano.scarfi@ingv.it

Citation:
Scarfì, L., Langer, H., Messina, A., & Musumeci, C. (2021). Tectonic regimes inferred from clustering of focal mechanisms and their distribution in space: application to the Central Mediterranean Area. *Journal of Geophysical Research: Solid Earth*, *126*, e2020JB020519. https://doi.org/10.1029/2020JB020519

Received 3 JUL 2020
Accepted 5 DEC 2020

Tectonic Regimes Inferred From Clustering of Focal Mechanisms and Their Distribution in Space: Application to the Central Mediterranean Area

L. Scarfì[1], H. Langer[1], A. Messina[2], and C. Musumeci[1]

[1]Istituto Nazionale di Geofisica e Vulcanologia, Catania, Italy, [2]Istituto Nazionale di Geofisica e Vulcanologia, Roma, Italy

Abstract The study of the kinematics and stress field related to seismicity makes an important contribution to the understanding of tectonic processes. In this kind of analysis, a crucial issue is identifying seismically homogeneous areas, which implies data classification and cluster creation. We present an approach that combines unsupervised learning techniques in order to reveal patterns in the focal mechanisms data set. In particular, a combination of two popular clustering algorithms, that is, self-organizing maps and Fuzzy C-means, was applied to focal mechanisms of events located in the Central Mediterranean region, characterized by a complex geodynamic framework. The analysis allowed identifying eight groups of focal mechanisms and their spatial distribution in the crust, and revealing the tectonic style of key sectors of southern Italy and of the neighboring offshore areas. A compressive regime was found between the lower Tyrrhenian Sea and southeastern Sicily, whereas extension prevails along the Calabrian Arc and the southern Apennines. A NW-SE transcurrent faulting between the Aeolian Islands and the Ionian Sea forms a transfer zone between these two domains.

Plain Language Summary The study of mechanisms describing the movement of the crustal blocks in a fault and of the forces causing earthquakes, provides precious information on the ongoing tectonic processes in a region. An important aspect in such an analysis is distinguishing the type of fault mechanism and identifying seismically homogeneous areas. To this end, in this work we have used a two-step approach that combines unsupervised learning—where objects are classified by the computer on the basis of their characteristics—and an analysis of the spatial distribution of the objects. This approach has been applied to a data set selected from the earthquakes recorded in the past 40 years in the Central Mediterranean region. The first step allowed distinguishing the earthquake mechanisms into fairly homogeneous groups; the final step was the analysis of their distribution in space, aiming at identifying prevailing regimes of deformation within the crust. In this way, we were able to characterize the different tectonic processes acting in key areas of the studied region.

1. Introduction

The spatial distribution of seismic energy radiated by an earthquake—often referred to as the "radiation pattern"—provides precious information on the forces acting in seismic sources and the orientation of rupture occurring during the event. The study of earthquake fault mechanisms reveals tectonic processes ongoing at depth, completing the picture inferred from field studies of the geologist which focus on the structures visible at the Earth's surface.

An important aspect in such analysis is distinguishing the type of earthquake mechanism. Here, we concentrate on double couple mechanisms, that is, seismic sources caused by pure shear fracturing, which by far dominate the seismic energy radiated worldwide. Using Anderson's classical scheme (Anderson, 1942), we identify three principal types of shear faulting: "Normal," "Reverse," and "Horizontal Strike-Slip" faulting, characterized by different orientation of the principal strain axes, that is, P, the axis of the maximum shortening, T, the one of the maximum extension, and B, the axis at the intersection of the nodal planes. Normal faulting mechanisms are characterized by a vertical orientation of the P-axis, while T is found parallel to the Earth's surface. In reverse faulting we see the opposite, the P-axis is horizontal and the T-axis is vertical. Finally, in strike-slip motion, pressure and tension axes are both oriented horizontally.

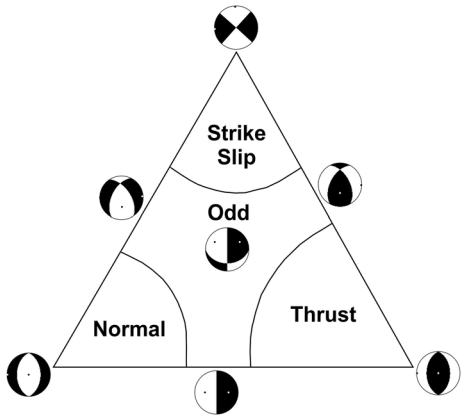

Figure 1. Focal mechanisms classification based on the plunge of P-, T-, and B-axes (following Frohlich & Apperson, 1992).

In reality, the picture resulting from the analysis of focal mechanisms is more complicated, there being a continuum of mixed mechanisms depending on the orientation of the strain axes and fault planes. A more comprehensive classification scheme has been proposed, for instance, by Frohlich and Apperson (1992) (see Figure 1). This classification, which includes mechanisms not attributable to any of the classic Anderson classes, is based on an a priori defined fields occupied by the P-, T-, and B-axes. Mechanisms close to vertices (Figure 1) are either predominantly normal, thrust or strike-slip; hybrid mechanisms are plotted in the central areas of the diagram.

Classification schemes like the one shown in Figure 1 have been implemented in models for empirical ground motion prediction equations (GMPE), for instance, in the formalism proposed by Boore and Atkinson (2008). In those models, the type of focal mechanism is accounted for by introducing a categorical vector composed of four Boolean values. Each entry represents a category. A horizontal strike slip is represented as (1 0 0 0), normal fault as (0 1 0 0), reverse fault as (0 0 1 0), unknown/odd as (0 0 0 1). Such a strategy implies having an a priori, user defined delineation of the four categories of mechanism. Besides, no information including the strike of axes is included in this scheme, which may be irrelevant in the context of GMPE but is a serious limitation in the study proposed here. Indeed, in tectonic studies we investigate the orientation of the stress field controlling the tectonic processes of an area and the analysis of focal mechanisms play a key role in this context. Stress orientation is inferred by assuming that the principal stress axes, $\sigma 1 > \sigma 2 > \sigma 3$, are expected to lie close to the P-, B-, and T-axes, respectively. Assuming that the slip of each earthquake occurs on a fault according to the direction of maximum shear stress, the basic approach of various techniques is to find a uniform stress tensor that minimizes the discrepancy between the predicted shear stress direction and the observed slip direction on each fault mechanism (e.g., Gephart & Forsyth, 1984; Michael, 1987). Local variations of stress field orientation in the lithosphere occur at a variety of scales and are caused both by the interaction of regional forces—related to the plate motions—and more local effects reflecting structure heterogeneities, such as differences of crustal loading or the presence of magmatic flows. Though in nature the transition between two different states of stress must be continuous, in seismology the usual practice is to divide a region into smaller subareas and independently fit a stress tensor to the focal mechanisms of each subarea. A key point of this approach is the identification of areas that can be considered homogeneous from a seismotectonic point of view. Wyss and Lu (1995) consider the deviation of individual fault-plane orientation with respect to a reference solution, typically given by fault a priori revealed in the field. Hardebeck and Michael (2006) and Martínez-Garzón et al. (2016) divide the space in a grid, whose dimensions should reflect seismic homogeneity. A common drawback of these techniques is that they require some a prior choices, such as how to bundle the input data (Hardebeck & Michael, 2004) or the identification of a degree of uniform seismicity when selecting the geometry of the grid. Indeed, overly small areas can result in unstable inversion; on the contrary, very large cells can group tectonically heterogeneous zones and some relevant stress variations may be lost. In order to resolve the problem, various authors have adopted clustering approaches with the aim of identifying families of events with similar source geometry, where the degree of similarity between two samples is based on some metric (Cesca et al., 2014; Willemann, 1993) rather than a priori defined ranges.

In this paper, we have applied several approaches of "unsupervised learning" to a data set of focal mechanisms calculated for earthquakes in southern Italy and in the neighboring offshore areas. These techniques—here the self-organizing maps (SOM) and the Fuzzy C-means (FCM)—use a metric of similarity between patterns rather than exploiting a priori defined target information furnished by an expert (see Supporting Information for more information about the techniques). Results show that the proposed procedure can represent an effective tool to study the kinematics, the stress regime and their variation in space.

2. Application in the Central Mediterranean

2.1. Tectonic Background

In the studied area, the long-lasting convergence between Eurasian and African Plates has led to the formation of a collisional and subduction complex, that includes fold-thrust belts and back-arc basins (e.g., Faccenna et al., 2004; van Hinsbergen et al., 2020; and references therein). In Figure 2, different tectonic domains are indicated. Moving from south to north, the main elements of the orogenic belt are the Sicilian Maghrebian Chain (SMC), the Calabro-Peloritan Arc (CPA), and the Apennines. The CPA is one of the sectors of maximum distortion of the orogenic belt facing the Mediterranean. It connects the NE-trending SMC and the NW-trending southern Apennines. The CPA origin is linked to the deformation of the European margin, whereas the SMC and the southern Apennines derive from the deformation of the African and the Adriatic microplate continental margins, respectively (e.g., see Billi et al., 2011 and references therein). The Pelagian block, which includes the continental crustal portion of the Hyblean Plateau in SE Sicily, and the Apulia Platform represent the foreland domains. During the late stage of crustal shortening (early Pleistocene), the outer margins of these forelands were involved in the thrust system and underplated at the base of the orogenic belt (Lentini et al., 2006). The geologic architecture of the region, seismicity, and magmatism are conditioned by the subduction of the denser oceanic Ionian lithosphere beneath the European margin. The current tectonic framework is the outcome of a complex evolution begun in the middle Miocene when a fast Ionian slab retrograde migration led to the opening of large back-arc extensional basins (i.e., Liguro-Provençal, Algerian, Alboran, and Tyrrhenian basins), as well as the lateral migration and relative rotation of orogenic wedges and foreland fragments and the retreat of trenches (see Faccenna et al., 2014). Subsequently, the subduction zone has become progressively narrower (Rosenbaum et al., 2008; Schellart et al., 2007); indeed, today it is confined between central Calabria and northeastern Sicily (see Scarfì et al., 2018).

The occurrence at the same time of ongoing collision (in Sicily) and subduction (beneath the CPA) with uneven deformation rates since Pliocene times led to the development of a transition zone between these two domains, characterized by roughly NW-SE trending dextral wrenching fault systems which extend to the Tyrrhenian Sea, NE Sicily, and the Ionian Sea. This boundary also decouples two main areas dominated by different kinematics: compressive to the west of the Aeolian Islands, and extensional to the east and northeast (e.g., Barreca et al., 2019; Scarfì et al., 2016; and reference therein).

2.2. Data set

The data set consists of focal mechanisms of earthquakes located in Southern Italy and in the neighboring offshore areas, taken both from catalogs (Pondrelli, 2002; Scarfi et al., 2013; Scognamiglio et al., 2006; Vannucci et al., 2003) and from published data in the literature (Anderson & Jackson, 1987; De Guidi et al., 2015; Frepoli et al., 2011; Giampiccolo et al., 2008; Maggi et al., 2009; Musumeci et al., 2014; Neri et al., 2004, 2005, 2003; Patanè & Privitera, 2001; Presti et al., 2013; Scarfi et al, 2016; Totaro et al., 2016). The shallow events of Etna volcano (depth <15 km) were excluded since they are related to specific fault systems that have developed in the context of the dynamics of the volcano rather than regional tectonic processes. Structural variations at narrow scales of a few kilometers, typical for the situation on Mt. Etna, require a separate and more detailed analysis.

In total, we collected a data set of 1,274 focal solutions (magnitude values mostly in the range $2 < M < 4$; maximum depth 60 km), which can be considered representative of the kinematics characterizing the seismically active areas of the region. Basically, these events cover a period from 1990 to 2017, but solutions of some moderate to large earthquakes (magnitude between 5 and 7) occurring in previous decades are also included (e.g., the 1908 Messina Strait event).

3. Clustering of Focal Mechanisms

3.1. SOM

SOM (Kohonen, 1984, 2001) are based on two key ideas: reduction of the number of input objects and reduction of the dimensionality of the problem. An object (or sample) is represented by an array of values,

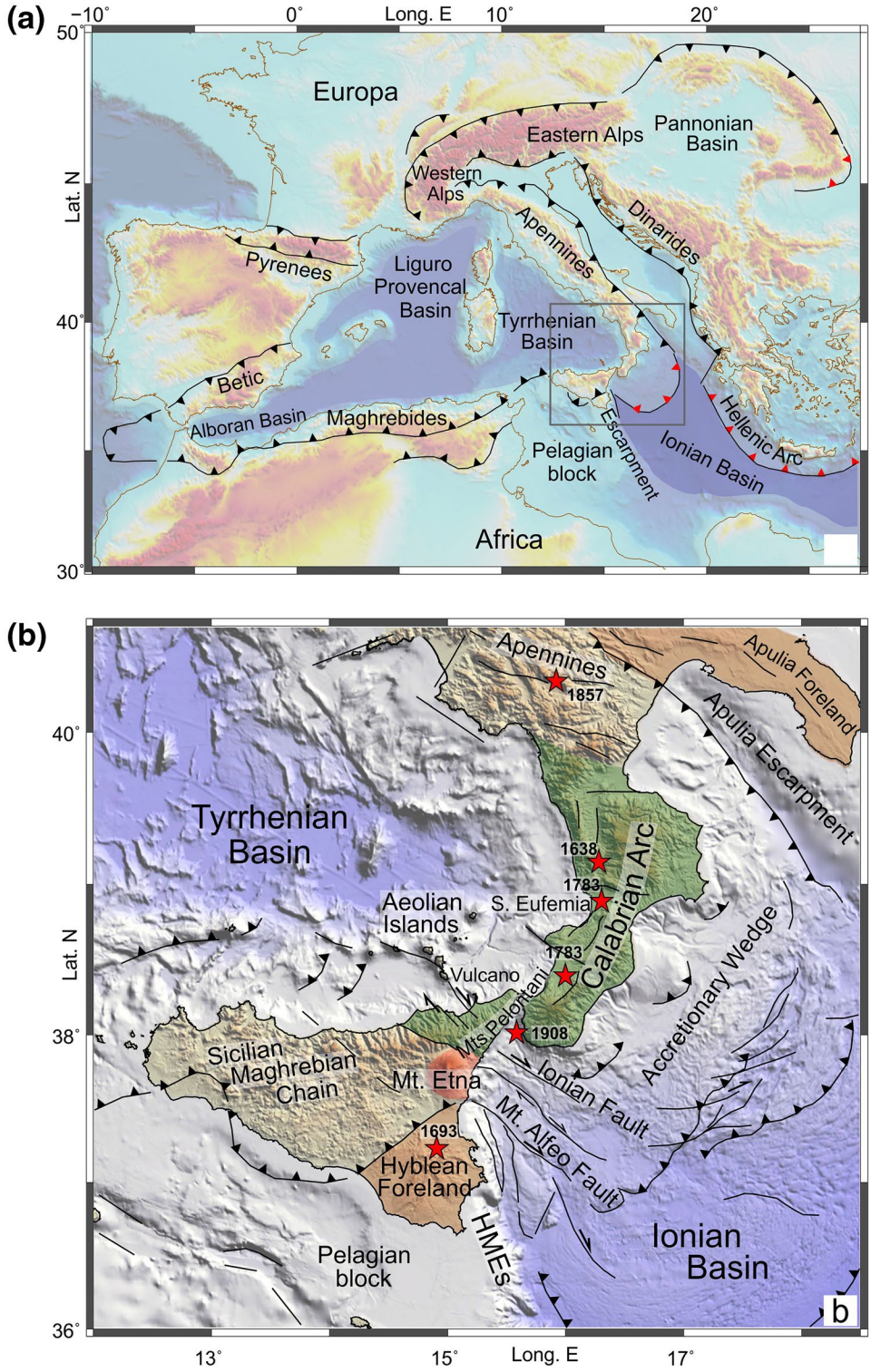

Figure 2. a) Map of the main orogenic belts, basins and subduction zones of the Mediterranean area. Triangles point in the direction of subduction or underthrusting; in red where the subducting slab is considered to be continuous. (b) Map showing the main geological and tectonic features of the studied region. Red stars indicate earthquake epicenters with $M > 7$ occurring during the last four centuries (Rovida et al., 2019). HMEs stand for Hyblean-Maltese Escarpment.

called feature vector. The goal is achieved by identifying a number of prototypes that represent our original data set with reasonable fidelity. These prototypes, still having the full dimensionality of the original data, are projected into a lower dimensionality representation space, here a two-dimensional (2D) map. In the end, we get a map of nodes, which can be understood as micro-clusters, each of which represents a number of input samples. The centroids of the micro-clusters, given as the average feature vector of the samples of a node, can be used as prototypes for these elements. Ideally, the topological relationships between samples are preserved: objects close to each other in the original data space will have close representations on the SOM. By applying a color code to the nodes depending on their position on the map, we are able to effectively represent the characteristics of a high dimensional data set just by plotting a 2D map made up of colored symbols.

Here, we have used SOM implemented in a modified version of the software package KKAnalysis (see Langer et al, 2020; Messina & Langer, 2011). A key issue was to establish the input features, that is, the representative characteristics of the items to be processed (in our case, focal mechanisms). The use of angles, indicating strike and plunge of the principal strain axes, comes with problems regarding a suitable definition of metrics describing the similarity of two patterns. For instance, strike directions of 5° and 355° differ by 10°, whereas the two values "5" and "355" differ by 350°. On the other hand, the two nodal planes of a shear type fault plane solution differ by 90°, even though they are equivalent in physical terms. We therefore adopted the six moment tensor components as input features since centroid-based clustering algorithms can deal with them in a straightforward way. Such an approach has recently been proposed by Langer et al. (2020), who considered moment tensors calculated for earthquakes with $M > 4$ in the Central Mediterranean area.

The algorithm grouped all the 1,274 focal solutions in 180 nodes (in reality 171, since 9 nodes do not contain elements; see Figure 3a). Figure 3b shows these solutions colored according to the SOM node membership. Neighboring nodes on the grid have similar colors, reflecting also objects with similar characteristics. Following the approach considered in Langer et al. (2020), the recognition of homogeneous groups of moment tensors can be carried out by culling together the elements of nodes with a similar color. However, even though Figure 3 shows the "similarity measures" of the input data set well, we are still dealing with a large number of prototypes (i.e., 171). Moreover, the identification of homogeneous groups following the strategy of considering nearby nodes needs an accurate visual inspection of the map and cannot be easily automated. The choice of samples to cull together on the map remains arbitrary to some degree, as we have no formal rule how to handle objects with transitional characteristics or being just noise, that is, which resemble only few or even no other events.

3.2. Fuzzy Clustering

To overcome SOM drawbacks we applied FCM clustering, which enables clustering both items with a strong similarity and elements whose characteristics are transitional or do not resemble other items at all. FCM (Bezdek, 1981; Dunn, 1973) is an unsupervised clustering algorithm that extends the Crisp C-means, better known as K-means (MacQueen, 1967). Differently from the latter, in fuzzy clustering every input element may belong to several clusters with different membership values. Consequently, the membership of an object to each of the M clusters is given by a M-dimensional vector, rather than an integer or Boolean value indicating an exclusive membership of the object to a cluster. Each component of the fuzzy membership vector expresses the degree to which the object belongs to a cluster. This is particularly useful when the boundaries among clusters are ambiguous, allowing a reasonable representation of the real-world situation characterized by the presence of uncertainty and imprecision. Objects for which one membership value clearly prevails over the rest are represented well by the centroid of that cluster. On the other hand, objects without a clearly prevailing membership are not well represented by either of the prototypes. Such elements have a position in the data space either lying between some centroids (transitional area) or are outliers, with very different characteristics with respect to all cluster centroids.

We performed the FCM clustering by exploiting the results obtained from the SOM. Specifically, the original moment tensors of the data set were replaced by the ones of the prototypes, being representative of the original items. This significantly reduced the scatter of the data; indeed, instead of having 1,274 different moment tensors the variability reduces to only 171 versions of feature vectors. The optimal number of

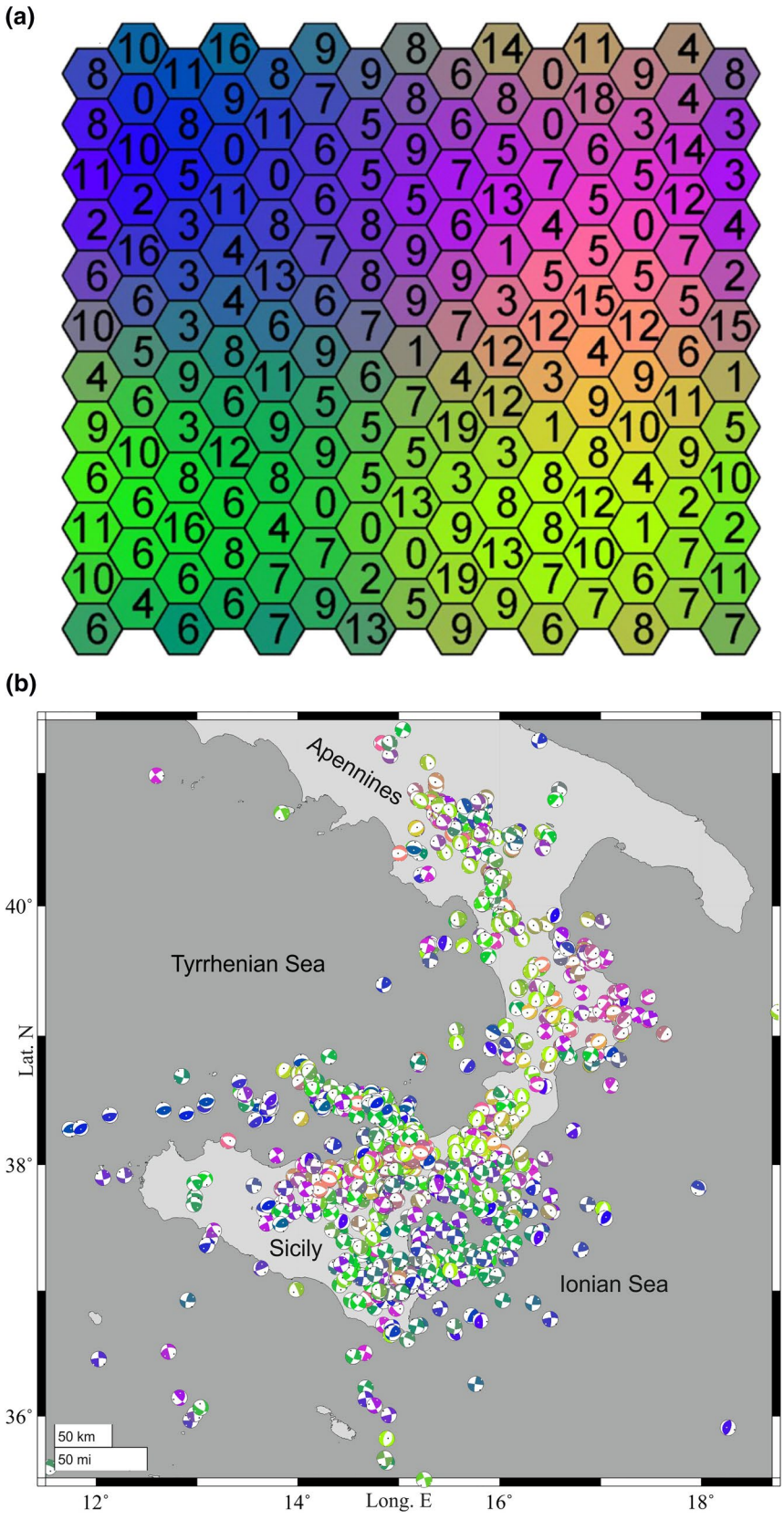

Figure 3. a) Distribution of nodes deriving from the SOM analysis, projected into a 2D map. Numbers indicate the moment tensors clustered in each node. (b) Focal mechanisms used in this study colored according to the SOM node membership. 2D, two-dimensional; SOM, self-organizing maps.

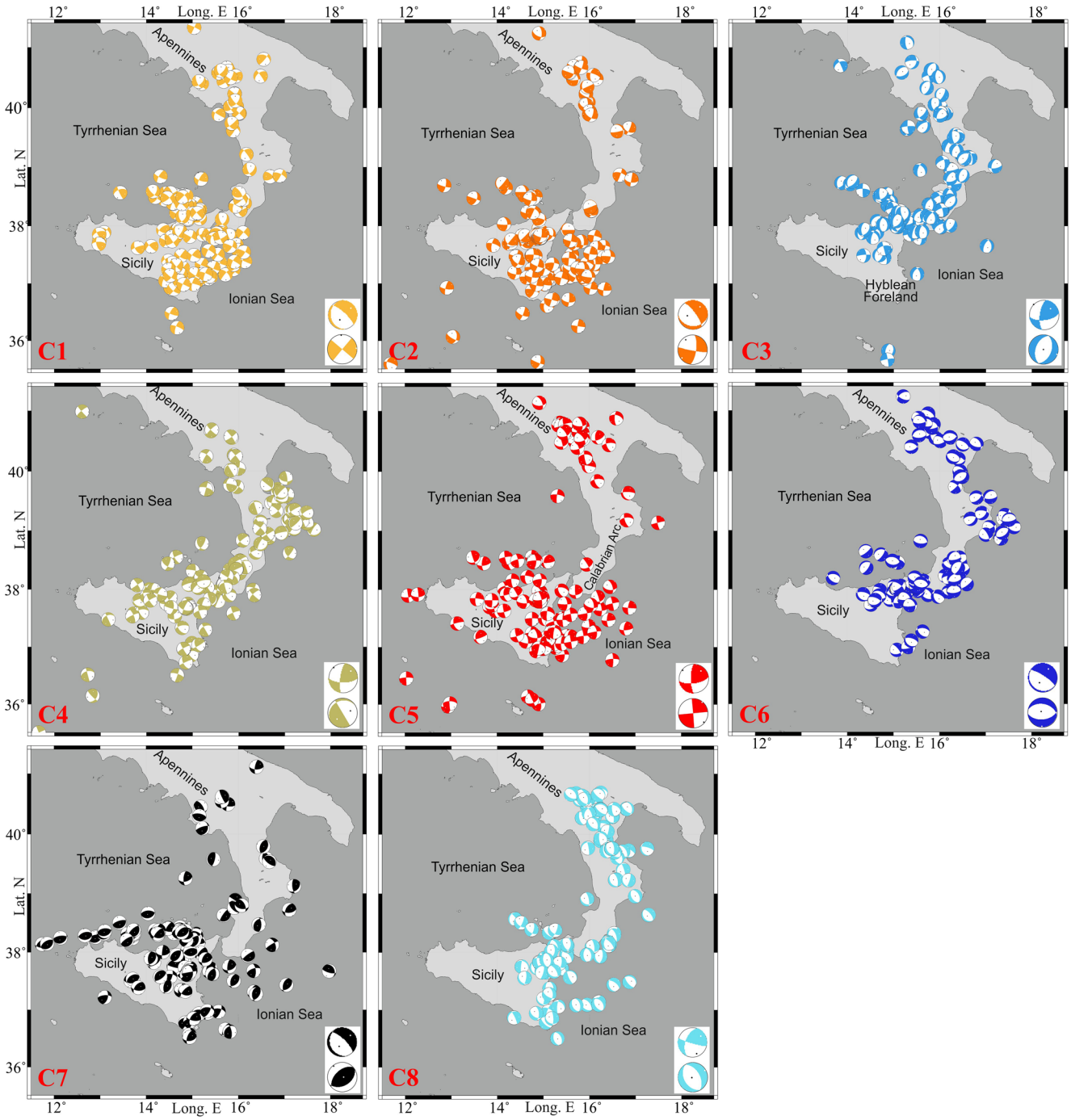

Figure 4. Groups of focal mechanisms derived from the FCM clustering (C1, ..., C8). On the right corner of the panels, the identified prototypes of each group are reported: top, by the calculation of the average moment tensor; bottom, by the Kagan angles (see text for further details). FCM, Fuzzy C-means.

partitions (clusters) of the data set was found by the Davies-Bouldin index (Davies & Bouldin, 1979), which provides a measure of the goodness of clustering. Based on this index, we have chosen to consider eight groups as being a reasonable compromise between the need for internal cluster homogeneity and data reduction. The results of the adopted clusterization are shown in Figure 4. For simplicity's sake, at this stage, we assign each focal mechanism to a cluster considering only its highest membership value. Note, however, that we will exploit the full cluster membership vectors in Chapter 4.

Table 1
Averaged Kagan Angles for the Most Representative Pattern of Each Cluster

Cluster	No. of members	Average Kagan angle
1	180	32.57
2	169	30.98
3	156	38.26
4	145	46.05
5	157	32.18
6	149	33.40
7	155	41.77
8	160	29.04

Even though the clusters are fairly well distinguished among each other, we may wish to summarize their overall characteristics. This is typically done by identifying the "prototypes," that is, patterns that are similar to all members of a cluster, thus being representative of it.

For identifying the typical mechanism, we have considered two options:

(i) Calculating the average moment tensor for each cluster and extracting its double couple part.
(ii) Calculating the Kagan angles (see Kagan, 2007) among all samples of the cluster and taking the pattern which has the lowest average angle with respect to all the other members.

As we have used the moment tensor components as feature vectors, one may be tempted just to use the average of the moment tensors for each cluster as proposed in option (i). In Figure 4 we indicate the nodal planes derived from this averaging (see the upper beach ball in the inset at the right corner of each panel). The alternative method of identifying prototypes exploits the Kagan angles. This metric is based on the angle by which a system P, T, B must be rotated so that the axes fall in the same position as P′, T′, B′ (see Supporting Information); it may vary from 0° (indicating a perfect match between the two solutions) to 120° (total mismatch). Therefore, we calculated the average Kagan angle of each cluster member with respect to all other elements of the same cluster. The most representative sample is the one with the lowest value (see Table 1 and the lower beach ball in the insets of the panels of Figure 4). From a visual inspection, we tend to prefer the second approach, as the representation obtained from the average moment tensor does not appear especially convincing. This can be understood from the fact that the sum of single double couple moment (DC) tensors do not automatically lead to a moment tensor representing again a double couple mechanism. In fact, other components, such as isotropic and CLVD ones, may be introduced and, as a consequence, the average solutions when extracting the DC part are distorted.

Kagan angles (Table 1) indicate that clusters are fairly homogeneous. In particular, clusters 1, 2, and 5 correspond essentially to horizontal strike slip mechanisms. They are distinguished by differences in the direction of the P-axis, which strikes N-S for the members of cluster 1, mainly NNW-SSE for those of cluster 2, and NW-SE for the samples belonging to the cluster 5. Clusters 3, 6, and 8 are characterized by a vertical P-axis and correspond to normal fault mechanisms. The three groups are differentiated between each other by the orientation of the B- and T-axes. Considering the B-axes, we find them more or less horizontal for the majority of the samples. Their orientation corresponds to the strike of the nodal planes mainly in a NE-SW direction (cluster 3), E-W (cluster 6), and NNW-SSE (cluster 8). Cluster 4 forms a fairly heterogeneous group with several horizontal strike slip mechanisms and P-axes directed in E-W, but also normal fault components are found. Indeed, in Table 1, cluster 4 is the one where the average Kagan angle of the prototype is the highest of all eight clusters. Finally, cluster 7 is also fairly homogeneous and reveals a compressive style, with P-axes mainly oriented in NW-SE direction.

4. Spatial Analysis

4.1. 3D Gridding

Even though the mechanisms form rather well-defined clusters, their distribution over the area may still lack clearly recognizable zones where a certain style of fault plane solutions prevails. In part, this can be expected from general tectonic considerations. Even along well-developed major fault systems, like the San Andreas Fault in California or the mid-oceanic rift systems, we notice secondary faults, which do not match, at first glance, the overall tectonic picture, but develop in the context of local stress changes. Indeed, dealing with small earthquakes, we need to be aware of the fact that these minor events represent both overall features of the tectonic processes as well as secondary minor elements that accompany the former. Besides, having so many samples in a restricted area poses problems of an efficient graphical representation. It becomes unavoidable that small groups appear overrepresented owing to the narrow spaces. A further

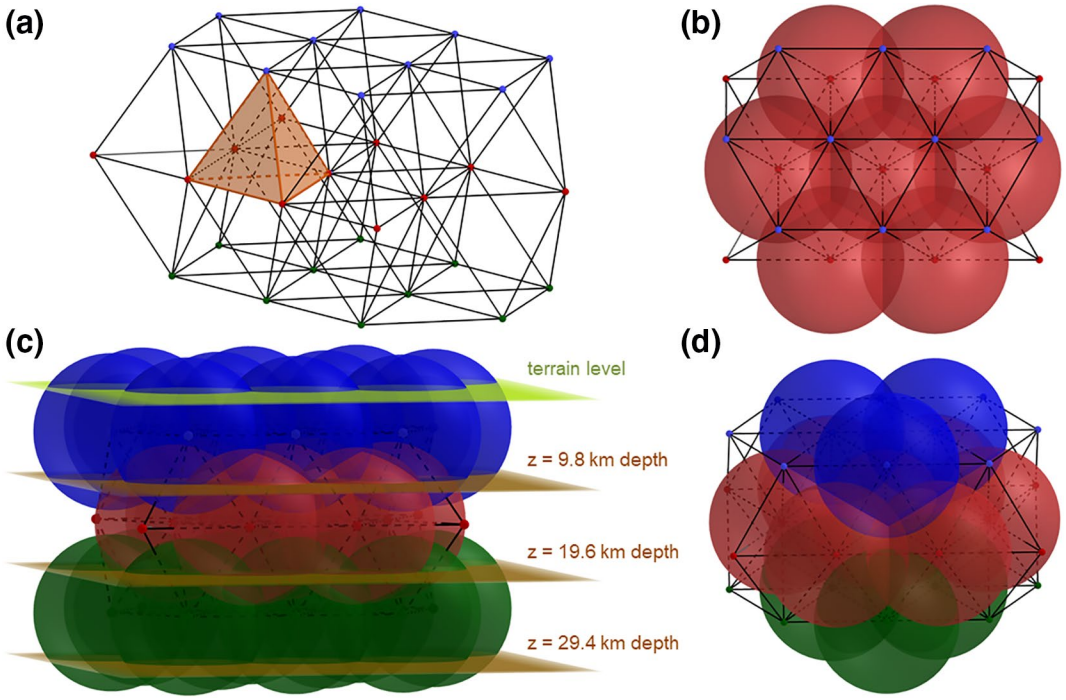

Figure 5. Geometry of the tetrahedral mesh (a) and of the spherical volumes sampling the crust (b) top view; (c and d) 3D view. 3D, three-dimensional.

aspect is the fact that epicenter maps represent marginal distributions, that is, a projection of 3D data to a presentation in a lower dimension, in this case maps. The problem of marginal distributions is well-known: structures in the high-dimensional data, such as separating elements or some geometric peculiarities of data groups, often appear blurred.

To preserve important characteristics of the spatial distribution of our data, we implemented a procedure to define the prevailing cluster memberships, within volumes of a certain extension both in horizontal and vertical directions. Specifically, we decided to partition the spatial domain by spherical volumes centered on the vertex of a regular tetrahedral mesh. This topology is known as "most dense packing" in crystallography. A regular tetrahedron is made up of four equilateral triangular faces and its four vertex corners are at the same distance from each other (Figure 5). The latter property cannot be obtained using other conventional gridding geometries, such as a mesh composed of cubes. Hence, the first step entails defining a grid structure, where each node is 12-km far from all the neighboring nodes, both on the same horizontal plane (same depth) as well as on adjacent planes (different depth). According to the tetrahedral structure, each horizontal layer is located 9.8 km from its neighboring planes. Finally, we obtained a grid consisting of 48 (longitudinal direction) × 73 (latitudinal direction) × 6 (vertical direction) nodes, covering depths ranging from 0 down to about 60 km.

Then, we designed n spheres having a radius of 8.5 km, centered in each node of the grid. The spherical shape allows to efficiently model the volume. In practice, all mechanisms within the spherical radius are associated with the respective node. Besides, considering the half-distance between nodes (6 km), the adoption of an 8.5 km radius for the spheres produces an overlap among neighboring volumes of 11.7% (Figure 5). The overlap introduces some kind of smoothing and mitigates the problem of boundary elements, that is, those items which fall near the border of a volume, far from its center. As an effect, during the regionalization phase, each clustered focal mechanism can fall into 1 (elements close to the center of a volume) to 4 discrete volumes (the most marginal ones). In our case, 46% of classified elements fell into two volumes, 28% in three, 24% in one, and only 2% in four volumes.

Once the grid is populated, the last step is to define the representative cluster for each not-empty volume. The algorithm for this operation is simple and straightforward; each grid node stores the number (K) of focal mechanisms allocated to it and a matrix of fuzzy membership values, consisting of K rows (one for each event) and M columns, where M is the number of clusters used in the classification step (see Table 2 as an example). As previously explained, each fuzzy membership value reports the degree to which a certain focal mechanism belongs to a cluster (information provided by FCM algorithm). Starting from the matrix of membership values stored in the grid node, a row vector is then calculated, containing the mean for each column (avg vector in Table 2). The highest mean value will define the most representative cluster for that node. Finally, a graphic representation of single horizontal layers was designed, plotting circles with a diameter of 12 km for each not-empty node. The circle reports the proxy cluster with the same color coding as used for the representation in Figure 4. Results for the four most meaningful layers are shown in Figure 6.

4.2. Results

Figure 6 provides an overview of the prevailing kinematics at various depth levels. In the shallower layer, down to about 10 km (Figure 6a), we observe a concentration of black nodes (indicating reverse faulting) in the southern Tyrrhenian Sea. Normal faulting with nodal planes striking NE (clusters 3) is present along most of the Calabro-Peloritan Arc, that is, in northeastern Sicily and central-southern Calabria; while moving toward the northern sector, nodes of cluster 8 are found, indicating a rotation of nodal planes in NW direction. The southern Apennines, the Aeolian Islands and central and southern Sicily are characterized by strike slip kinematics (clusters 1, 2, and 5), with N to NW P-axes oriented. Figure 6b is related to the events falling in a depth range 9.8–19.6 km. In this layer we note a strong presence of nodes representing horizontal strike slip motion in the Aeolian Islands sector (mainly cluster 1) and southern Sicily. Again, along the Calabro-Peloritan Arc and Southern Apennines, normal faulting with nodal planes striking according to the axes of these mountain ranges prevails. Normal mechanisms are also observed in the northern part of Sicily. In the central part of Calabria along the eastern coast, elements belonging to cluster 4, mostly corresponding to horizontal strike slip mechanisms with P-axes directed E-W, mark a line with NW-SE orientation. This last feature is also observed in the layer between 19.6 and 29.4 km (see Figure 6c). In addition, this depth interval is characterized by elements of clusters 1, 2, and 5 (horizontal strike slip mechanisms) which dominate in central-eastern Sicily, in the Ionian Sea and in the Aeolian Islands area. In other sectors we cannot recognize prevailing types of fault plane solutions; normal faulting with varying orientation of the axes are noticed together with horizontal strike slip motions and reverse faulting.

In the deepest layer considered here (depth range between 29.4 and 39.2 km, see Figure 6d), we can highlight two main areas: nodes indicating horizontal strike slip mechanisms, along a NW-SE direction in the Ionian offshore south of Calabria, and normal faults at the northern tip of this lineament, in northeastern Sicily.

In Figure 7 we attempt a simplified interpretation of the results discussed so far. In a map view we delimit sectors being as homogeneous as possible with respect to the tectonic regime. Some variability in the orientation of P- and T-axes is observed in some regions, for example, in the regions “B," “C,” and “D." Also in southern Calabria (region “F”), the type and orientation of faults show considerable differences among each other. In the remaining regions the tectonic regimes turn out rather homogeneous. It is also interesting to note that the prevailing kinematics of the various zones is consistent with the those shown by focal mechanisms for events with magnitude > 4.5.

In conclusion, some clues on the stress acting in the region can be inferred. We clearly identify a W-E compressive belt in the southern Tyrrhenian Sea, characterized by ENE-WSW reverse mechanisms, and an extensional deformation, perpendicular to mountain ranges, that characterizes the eastern sector of the studied area (i.e., NE Sicily, Calabrian Arc, and southern Apennines). We also recognize a transition zone between these two domains occurring in the Aeolian Islands area, where strike-slip kinematics with roughly N-S P-axis prevails. Overall, the area between the Aeolian Islands and the Ionian Sea depicts a NW-SE right transtensional zone, which is believed to be the shallow expression of a lithospheric-scale tear faults system located at the southern Ionian slab edge (e.g., Barreca et al., 2014, 2019; Scarfì et al., 2016, 2018).

Table 2
Example of Fuzzy Membership Matrix Stored in a Grid Node

Item number	Fuzzy clust. 1	Fuzzy clust. 2	Fuzzy clust. 3	Fuzzy clust. 4	Fuzzy clust. 5	Fuzzy clust. 6	Fuzzy clust. 7	Fuzzy clust. 8
1	0.0359	0.0788	0.0421	0.1698	0.4401	0.0982	0.0795	0.0558
2	0.0701	0.0915	0.0542	0.1286	0.1181	0.0588	0.4267	0.0520
3	0.0489	0.0727	0.0295	0.0570	0.0846	0.0319	0.6434	0.0319
4	0.0568	0.4362	0.0324	0.0368	0.2548	0.0392	0.0799	0.0638
5	0.0213	0.0299	0.0418	0.6772	0.0568	0.1016	0.0374	0.0339
6	0.0570	0.0906	0.0464	0.1249	0.1420	0.0597	0.4315	0.0479
Averaged vector	0.0483	0.1333	0.0411	0.1991	0.1827	0.0649	0.2831	0.0476

Note. The matrix reports the degree of membership to a cluster for six moment tensors, each represented by a fuzzy membership vector (row). The last row shows the averaged vector for all the six elements. In red, the highest value identifying the most representative cluster (see text for further explanation).

Most of Sicily, between the northern coastal mountain chain and the southernmost area, is characterized by mechanisms of clusters 1, 2, and 5, that is, strike-slip mechanisms with NW-SE to N-S striking P-axes, and several reverse mechanisms belonging to cluster 7. This pattern suggests an active compressive deformation in central and eastern Sicily, fitting well with the current compressive regime along the southern Tyrrhenian zone, which extends also into the Hyblean Foreland.

The overview provided by Figure 7 is consistent with findings found in recent general studies (e.g., Soumaya et al., 2015; Totaro et al., 2016) and highlights local perturbations of the first-order stress field. These can be attributed to the presence of major tectonic elements causing reorientations of the principal stress axes.

The extensional kinematics characterizing the coastal Tyrrhenian onshore appears incompatible at first glance with such a north-to-south compression. However, a careful analysis (see also Figure 6) reveals that most of the events with an extensional kinematics are localized at depth of less than about 20 km, while several solutions of deeper events have a subhorizontal P-axis. This can be explained considering various processes, such as upper crustal stretching above an active thrust belt (Lavecchia et al., 2007). Another explanation may be the presence of isostatic rebound due to the detachment of the slab or even the reactivation of pre-existing faults under the impulse of an upwelling of melt mantle material beneath Mt. Etna (Billi et al., 2010). In all cases, the main regime to the west and southwest of the Aeolian Islands appears to accommodate the Africa-Europa convergence.

Southern Italy, from Calabria to the Messina Strait, primarily exhibits normal faulting along the axial part of the chain; however, adjacent crustal domains are characterized by transcurrent regimes. In particular, main strike-slip kinematics along a roughly NW-SE trend is recognized in central-eastern Calabria, broadly overlapping the so-called Pollino Line. It is a shear zone with tensional and compressional components (e.g., Ferranti et al., 2017), which could be a shallow tectonic feature of a residual retrograde movement at the edge of the Ionian slab fragment (e.g., Palano et al., 2017). Strike-slip movement with NW-SE trending P-axes is also found in the southern Apennines.

5. Conclusion

In the data set considered, we face a complex situation linked to the very specific geological and tectonic structure in Southern Italy, where various geodynamic processes interact. The considerable number of focal mechanisms—over 1,200 in total—and the high dimensionality of the data (six moment tensor components or corresponding angular values for nodal planes or stress axes) pose severe problems for a visual analysis of data structures and in separating elements. By applying clustering, we seek to identify structures in a data set, being they groups or heterogeneity. A key point of these techniques is that no a priori information is necessary for this task besides the definition of a metric expressing similarity among patterns.

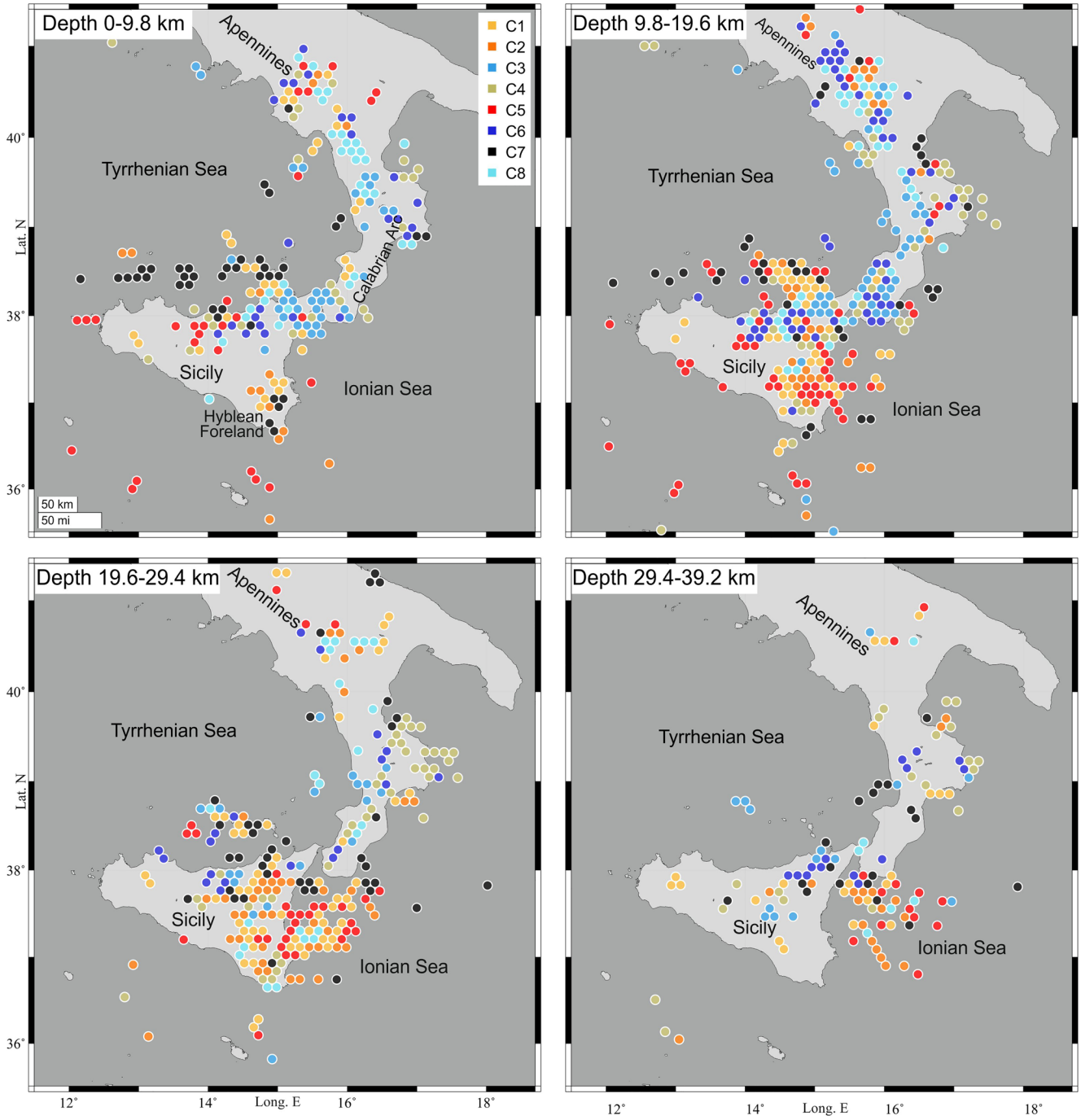

Figure 6. Layers at different depths showing the 3D grid not-empty volumes sampling the moment tensors data set. Color code is the same as used in Figure 4; it indicates the representative cluster for each volume. 3D, three-dimensional.

Here, we have applied a combination of two popular clustering algorithms, that is, SOM and FCM. Both techniques apply well to regimes with clearly developed clusters as well transitional regimes, where pattern characteristics imply a mixture and assignment to one group exclusively is inappropriate. SOM allows identifying a number of representative prototypes for the original data, which is still sizable, but introduces some smoothing and therefore simplifies the classification problem. Mapping the prototypes to a 2D representation enables an effective visualization of the similarities encountered between the patterns as similar patterns have positions close to each other on the map. We can also describe the position on the map by a

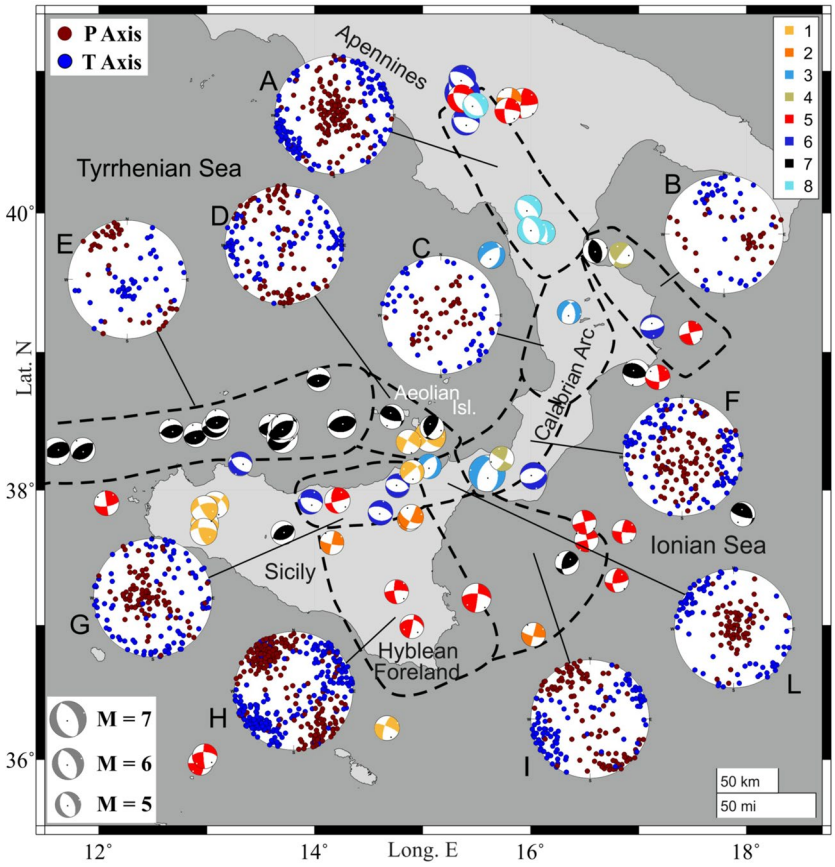

Figure 7. Distribution of the P- and T-axes of the focal mechanisms comprised in the areas identified by the dotted lines. Focal mechanisms of the earthquakes with $M > 4.5$ are also shown; color code is the same as used in Figure 4.

color code which further facilitates visualization. The analysis of the map clearly illustrates the variety of existing mechanisms; in addition, it provides a rough idea of macro groups with very similar features. Still, we are left with a considerable number of prototypes, and the delineation of macro groups on the map requires visual inspection. In order to further formalize the classification, we processed the results of the SOM using the FCM algorithm. Thus, we were able to analytically group all the focal solutions into eight clusters with a reasonable degree of homogeneity (i.e., low Kagan angles among the elements of each group).

The final step was the analysis of the 3D distribution of the focal mechanisms. In order to identify prevailing stress regimes within the crust, we applied a partitioning of the whole crust through spherical volumes of adequate size. Each of these volumes was categorized according to the prototype of the group of focal mechanisms that proved the most representative after the weighting of the cluster membership degrees of all the focal mechanisms inside the volume. In this way, we were able to characterize the kinematics of the area and obtain indications of stress orientation and its variation in space.

In essence, we recognize a substantially compressive regime (P axes striking roughly NW-SE) between the lower Tyrrhenian Sea—marked by the occurrence of reverse faulting—and southeastern Sicily with prevailing horizontal strike-slip mechanisms. On the other hand, extension prevails along the southern Apennines, Calabria, and Peloritani Mts. NW-SE dextral strike-slip motion between Aeolian Islands and the Ionian Sea forms a transfer zone between these two domains. Interestingly, the picture also highlights a strike-slip regime in Calabria and a superficial regime of extension in the Tyrrhenian onshore zone of Sicily.

We see a major advantage of our application in that—being based on unsupervised learning techniques—only a very limited amount of a priori information is required. This regards the choice of the metric, the topology of the SOM and its size. The number of clusters has to be defined a priori, but it can be derived

from automatically defined criteria, such as the Davies-Bouldin index. The strategy outlined in our work can thus also be applied in other areas where a sufficient number of good quality focal mechanism is available.

Conflict of Interest

The authors declare that they have no known competing financial interests or personal relationships that could have appeared to influence the work reported in this paper.

Data Availability Statement

All the analyzed data and tools are available in literature. In particular, the focal solutions were taken from catalogs (Pondrelli, 2002; Scarfi et al., 2013; Scognamiglio et al., 2006; Vannucci et al., 2003) and published data (Anderson & Jackson, 1987; De Guidi et al., 2015; Frepoli et al., 2011; Giampiccolo et al., 2008; Maggi et al., 2009; Musumeci et al., 2014; Neri et al, 2004, 2005, 2003; Patanè & Privitera, 2001; Presti et al., 2013; Scarfi et al, 2016; Totaro et al., 2016). The software package KKAnalysis is available at the companion website of Langer et al. (2020): https://www.elsevier.com/books-and-journals/book-companion/9780128118429.

Acknowledgment
The authors wish to thank Steve Conway for his review regarding the use of English and two anonymous reviewers for their constructive and helpful suggestions.

References

Anderson, E. M. (1942). *The dynamics of faulting and dyke formation with applications to Britain*. London: Oliver and Boyd.
Anderson, H., & Jackson, J. (1987). The deep seismicity of the Tyrrhenian Sea. *Geophysical Journal International*, *91*(3), 613–637.
Barreca, G., Bruno, V., Cultrera, F., Mattia, M., Monaco, C., & Scarfì, L. (2014). New insights in the geodynamics of the Lipari–Vulcano area (Aeolian Archipelago, southern Italy) from geological, geodetic and seismological data. *Journal of Geodynamics*, *82*, 150–167.
Barreca, G., Scarfì, L., Gross, F., Monaco, C., & De Guidi, G. (2019). Fault pattern and seismotectonic potential at the south-western edge of the Ionian subduction system (southern Italy): New field and geophysical constraints. *Tectonophysics*, *761*, 31–45.
Bezdek, J. C. (1981). *Pattern recognition with fuzzy objective functions algorithms*. New York, NY: Plenum Press (Springer). https://doi.org/10.1007/978-1-4757-0450-1
Billi, A., Faccenna, C., Bellier, O., Minelli, L., Neri, G., Piromallo, C., et al. (2011). Recent tectonic reorganization of the Nubia-Eurasia convergent boundary heading for the closure of the western Mediterranean. *Bulletin de la Société Géologique de France*, *182*, 279–303.
Billi, A., Presti, D., Orecchio, B., Faccenna, C., & Neri, G. (2010). Incipient extension along the active convergent margin of Nubia in Sicily, Italy: Cefalù-Etna seismic zone. *Tectonics*, *29*, TC4026.
Boore, D. M., & Atkinson, G. M. (2008). Ground-motion prediction equations for the average horizontal component of PGA, PGV, and 5%-damped PSA at spectral periods between 0.01 s and 100 s. *Earth Spectra*, *24*, 99–138.
Cesca, S., Sen, A. T., & Dahm, T. (2014). Seismicity monitoring by cluster analysis of moment tensors. *Geophysical Journal International*, *196*, 1813–1826.
Davies, D. L., & Bouldin, D. W. (1979). A cluster separation measure. *IEEE Transactions on Pattern Recognition and Machine Learning*, *1*(2), 224–227.
De Guidi, G., Barberi, G., Barreca, G., Bruno, V., Cultrera, F., Grassi, S., et al. (2015). Geological, seismological and geodetic evidence of active thrusting and folding south of Mt. Etna (eastern Sicily): Revaluation of "seismic efficiency" of the Sicilian Basal Thrust. *Journal of Geodynamics*, *90*, 32–41.
Dunn, J. C. (1973). A fuzzy relative of the ISODATA and its use in the detecting compact well deparated clusters. *Journal of Cybernetics*, *3*, 32–57.
Faccenna, C., Becker, T. W., Auer, L., Billi, A., Boschi, L., Brun, J. P., et al. (2014). Mantle dynamics in the Mediterranean. *Reviews of Geophysics*, *52*, 283–332.
Faccenna, C., Piromallo, C., Crespo-Blanc, A., Jolivet, L., & Rossetti, F. (2004). Lateral slab deformation and the origin of the western Mediterranean arcs. *Tectonics*, *23*, TC1012.
Ferranti, L., Milano, G., & Pierro, M. (2017). Insights on the seismotectonics of the western part of northern Calabria (southern Italy) by integrated geological and geophysical data: Coexistence of shallow extensional and deep strike-slip kinematics. *Tectonophysics*, *721*, 372–386.
Frepoli, A., Maggi, C., Cimini, G. B., Marchetti, A., & Chiappini, M. (2011). Seismotectonic of southern Apennines from recent passive seismic experiments. *Journal of Geodynamics*, *51*(2–3), 110–124.
Frohlich, C., & Apperson, K. D. (1992). Earthquake focal mechanisms, moment tensors, and the consistency of seismic activity near plate boundaries. *Tectonics*, *11*, 279–296.
Gephart, J. W., & Forsyth, D. W. (1984). An improved method for determining the regional stress tensor using earthquake focal mechanism data: Application to the San Fernando earthquake sequence. *Journal of Geophysical Research*, *89*, 9305–9320.
Giampiccolo, E., Musumeci, C., Falà, F., & Gresta, S. (2008). Seismological investigations in the Gioia Tauro basin (southwestern Calabria, Italy). *Annals of Geophysics*, *51*(5/6), 769–799.
Hardebeck, J. L., & Michael, A. J. (2004). Stress orientations at intermediate angles to the San Andreas Fault, California. *Journal of Geophysical Research*, *109*, B11303.
Hardebeck, J. L., & Michael, A. J. (2006). Damped regional-scale stress inversions: Methodology and examples for Southern California and the Coalinga aftershock sequence. *Journal of Geophysical Research*, *111*, B11310.
Kagan, Y. Y. (2007). Simplified algorithm for calculating double-couple rotation. *Geophysical Journal International*, *171*, 411–418.
Kohonen, T. (1984). *Self-organizing and associative memory, Springer Series in Information Sciences* (1st ed.,*8*). Berlin-Heildeberg-New York: Springer-Verlag.
Kohonen, T. (2001). *Self-organizing maps, Springer Series in Information Sciences* (3rd ed., *30*). Berlin, Germany: Springer-Verlag.

Langer, H., Falsaperla, S., & Hammer, C. (2020). *Advantages and pitfalls of pattern recognition: Selected cases in geophysics. Computational geophysics* (p. 350). Elsevier.

Lavecchia, G., Ferrarini, F., De Nardis, R., Visini, F., & Barbano, M. S. (2007). Active thrusting as a possible seismogenic source in Sicily (southern Italy): Some insights from integrated structural-kinematic and seismological data. *Tectonophysics*, *445*, 145–167.

Lentini, F., Carbone, S., & Guarnieri, P. (2006). Collisional and postcollisional tectonics of the Apenninic-Maghrebian orogen (southern Italy). In Y. Dilek & S. Pavlides (Eds.), *Postcollisional tectonics and magmatism in the Mediterranean region and Asia* (*429*, pp. 57–89). Boulder, CO: Geological Society of America.

MacQueen, J. (1967). Some methods for classification and analysis of multivariate observations. *Proceedings of the Fifth Berkeley Symposium on Mathematical Statistics and probability, Volume 1: Statistics* (pp. 281–297). Berkeley, CA: University of California Press.

Maggi, C., Frepoli, A., Cimini, G. B., Console, R., & Chiappini, M. (2009). Recent seismicity and crustal stress field in the Lucanian Apennines and surrounding areas (southern Italy): Seismotectonic implications. *Tectonophysics*, *463*, 130–144.

Martínez-Garzón, P., Ben-Zion, Y., Abolfathian, N., Kwiatek, G., & Bohnhoff, M. (2016). A refined methodology for stress inversions of earthquake focal mechanisms: Refined stress inversion methodology. *Journal of Geophysical Research*, *121*(12), 8666–8687.

Messina, A., & Langer, H. (2011). Pattern recognition of volcanic tremor data on Mt. Etna with KKAnalysis—A software program for unsupervised classification. *Computer and Geosciences*, *37*(7), 953–961.

Michael, A. J. (1987). Use of focal mechanisms to determine stress: A control study. *Journal of Geophysical Research*, *92*, 357–368.

Musumeci, C., Scarfì, L., Palano, M., & Patanè, D. (2014). Foreland segmentation along an active convergent margin: New constraints in southeastern Sicily (Italy) from seismic and geodetic observations. *Tectonophysics*, *630*, 137–149.

Neri, G., Barberi, G., Oliva, G., & Orecchio, B. (2004). Tectonic stress and seismogenic faulting in the area of the 1908 Messina earthquake, south Italy. *Geophysical Research Letters*, *31*, L10602. https://doi.org/10.1029/2004GL1019742

Neri, G., Barberi, G., Oliva, G., & Orecchio, B. (2005). Spatial variations of seismogenic stress orientations in Sicily, south Italy. *Physics of the Earth and Planetary Interiors*, *148*, 175–191.

Neri, G., Barberi, G., Orecchio, B., & Mostaccio, A. (2003). Seismic strain and seismogenic stress regimes in the crust of the southern Tyrrhenian region. *Earth and Planetary Science Letters*, *213*, 97–112.

Palano, M., Piromallo, C., & Chiarabba, C. (2017). Surface imprint of toroidal flow at retreating slab edges: The first geodetic evidence in the Calabrian subduction system. *Geophysical Research Letters*, *44*, 845–853.

Patanè, D., & Privitera, E. (2001). Seismicity related to 1989 and 1991-93 Mt. Etna (Italy) eruptions: Kinematic constraints by FPS analysis. *Journal of Volcanology and Geothermal Research*, *109*, 77–98.

Pondrelli, S. (2002). *European-Mediterranean Regional Centroid-Moment Tensors Catalog (RCMT) [Data set]. Istituto Nazionale di Geofisica e Vulcanologia (INGV)*. https://doi.org/10.13127/rcmt/euromed

Presti, D., Billi, A., Orecchio, B., Totaro, C., Faccenna, C., & Neri, G. (2013). Earthquake focal mechanisms, seismogenic stress, and seismotectonics of the Calabrian Arc, Italy. *Tectonophysics*, *602*, 153–175.

Rosenbaum, G., Gasparon, M., Lucente, F. P., Peccerillo, A., & Miller, M. S. (2008). Kinematics of slab tear faults during subduction segmentation and implications for Italian magmatism. *Tectonics*, *27*, TC2008.

Rovida, A., Locati, M., Camassi, R., Lolli, B., & Gasperini, P. (2019). *Catalogo Parametrico dei Terremoti Italiani (CPTI15), versione 2.0. Istituto Nazionale di Geofisica e Vulcanologia (INGV)*. https://doi.org/10.13127/CPTI/CPTI15.2

Scarfì, L., Barberi, G., Barreca, G., Cannavò, F., Koulakov, I., & Patanè, D. (2018). Slab narrowing in the Central Mediterranean: The Calabro-Ionian subduction zone as imaged by high resolution seismic tomography. *Scientific Reports*, *8*, 5178.

Scarfì, L., Barberi, G., Musumeci, C., & Patanè, D. (2016). Seismotectonics of northeastern Sicily and southern Calabria (Italy): New constraints on the tectonic structures featuring in a crucial sector for the Central Mediterranean geodynamics. *Tectonics*, *35*, 812–832.

Scarfì, L., Messina, A., & Cassisi, C. (2013). Sicily and southern Calabria focal mechanism database: A valuable tool for the local and regional stress field determination. *Annals of Geophysics*, *56*, 1.

Schellart, W. P., Freeman, J., Stegman, D. R., Moresi, L., & May, D. (2007). Evolution and diversity of subduction zones controlled by slab width. *Nature*, *446*, 308–311.

Scognamiglio, L., Tinti, E., & Quintiliani, M. (2006). *Time Domain Moment Tensor [Data set]. Istituto Nazionale di Geofisica e Vulcanologia (INGV)*. https://doi.org/10.13127/TDMT

Soumaya, A., Ben Ayed, N., Delvaux, D., & Ghanmi, M. (2015). Spatial variation of present-day stress field and tectonic regime in Tunisia and surroundings from formal inversion of focal mechanisms: Geodynamic implications for central Mediterranean. *Tectonics*, *34*, 1154–1180.

Totaro, C., Orecchio, B., Presti, D., Scolaro, S., & Neri, G. (2016). Seismogenic stress field estimation in the Calabrian Arc region (south Italy) from a Bayesian approach. *Geophysical Research Letters*, *43*, 8960–8969. https://doi.org/10.1002/2016GL070107

van Hinsbergen, D. J. J., Torsvik, T. H., Schmid, S. M., Maţenco, L. C., Maffione, M., Vissers, R. L. M., et al. (2020). Orogenic architecture of the Mediterranean region and kinematic reconstruction of its tectonic evolution since the Triassic. *Gondwana Research*, *81*, 79–229.

Vannucci, G., & Gasperini, P. (2003). A database of revised fault plane solutions for Italy and surrounding regions. *Computers & Geosciences*, *29*, 903–909.

Willemann, R. J. (1993). Cluster analysis of seismic moment tensor orientations. *Geophysical Journal International*, *115*(3), 617–634.

Wyss, M., & Lu, Z. (1995). Plate boundary segmentation by stress directions: Southern San Andreas Fault, California. *Geophysical Research Letters*, *22*, 547–550.